Density Functional Studies of Hydrogen Atom Addition to the C═S Bond

Roderick M. Macrae* and Ian Carmichael

Radiation Laboratory, University of Notre Dame, Notre Dame, Indiana 46556

Received: November 10, 2000; In Final Form: January 29, 2001

The results of density functional theory calculations on the structures, energetics, and hyperfine properties of radical H adducts to the C and S atoms of several thioketones and related species are presented. Despite the greater thermochemical stability of the C adduct in several cases, the isotropic proton couplings (and, where data are available, ^{14}N couplings) make it clear that the species observed in μSR experiments are S adducts, counter to the assignments made by the experimentalists. The preference for S addition is probably a result of the barrier associated with the geometrical distortion required for addition at C or may indicate a formation mechanism involving a charged intermediate. The distribution of the magnitudes of the couplings of both C and S adducts shows that previous intuitive arguments are inadequate in the assignment of experimental data. Calculation of the dynamically averaged temperature-dependent coupling within a one-mode approximation corrected for zero-point bond stretching yields almost-quantitative agreement with experiment for thioacetamide assuming addition is to S.

1. Introduction

The addition of H atoms across C═O and C═S bonds is a common route to the generation of free radicals, at least ostensibly.[1,2] (The actual route may be ionic, or the final product may derive from the fragmentation of a larger system.) The general consensus is that in the case of addition to the carbonyl group, addition at O is generally favored both thermodynamically and kinetically,[1,3] although the relative thermodynamic stabilities of C and O adducts in R_1R_2CO is dependent on the nature of the functional groups R_1 and R_2. In cases where the C adduct is more stable, it can be formed subsequently via isomerization; for example, the interconversion between the hydroxymethyl and methoxy radicals is an important aspect of atmospheric chemistry. In the case of C═S, on the other hand, orbital energy and size considerations suggest that addition to C to form a thiyl radical should be strongly favored energetically, and it is generally assumed that this will be the adduct produced in H atom isotope reactions despite the large barrier associated with addition at the trigonal center and transition to a tetrahedral geometry.[2,4] Thiyl radicals are of course of considerable importance in biology where they are formed by H atom abstraction from thiols, themselves act as H atom acceptors which repair free radical damage to biomolecules, and additionally participate in nitrosylation and oxidation processes.[5−7] Direct experimental means of observing these radicals are therefore paramount. The radicals are, however, in general difficult to observe by conventional ESR in fluid solution, although they are seen at low temperature in matrices. This is thought to be a result of the near-degeneracy of the π_x and π_y levels inherited from the prototype sulfanyl radical SH (see, for example, ref 8) and which leads to the Jahn−Teller distortion in $CH_3S^{\bullet}$;[9,10] dynamical averaging of a highly anisotropic *g*-tensor leads to extremely broad spectra. Variants of the muon spin rotation (μSR) technique, in which the place of atomic hydrogen is taken by its light isotope muonium, have however detected radicals formed by addition to C═S in liquids,[2,4,11−13] and from general considerations such as the assumption (supported by semiempirical calculations) that the C adduct is more stable and the rather large size of the hyperfine coupling as compared to couplings obtained in carbonyl systems (hundreds rather than tens of MHz[14]) the observed signals have been almost globally assigned to S-centered thiyl radicals from Mu addition at C. The one exception is the adduct radical to $(Ph)_2CS$, where the low muon coupling (equivalent to $A_p \sim 21.7$ MHz at 298 K[2]) is taken as evidence that addition in this case is to S, with a case being reasoned out for this conclusion in terms of electronic inductive effects.

In this paper, we argue from the results of B3LYP hybrid density functional calculations (recently shown to be accurate for the determination of hyperfine properties of S-containing radicals,[15] and which can give acceptable values for ^1H couplings even with a relatively small basis set[16]) that no simple magnitude-based rule of thumb can be adduced for the proton (muon) couplings in these systems, with S adducts and C adducts both leading to a wide range of A_p values depending on substituent, and hence that many of the assignments in the literature (and conclusions therefrom) may be in need of reconsideration.

2. Computational Methods

"Hybrid" density functional methods modify the density functional approximations to the exchange-correlation energy with an admixture of Hartree−Fock exchange. All the calculations presented here use the B3LYP functional, which embodies Becke's three-parameter expression for the exchange-correlation energy

$$E_X = aE_X^{\text{Slater}} + (1-a)E_X^{\text{HF}} + bE_X^{\text{Becke}} + cE_C^{\text{LYP}} + (1-c)E_C^{\text{VWN}} \quad (1)$$

obtained by fitting atomization energies and other properties for the G1 molecule set.[17] More recently, other hybrid func-

* To whom correspondence should be addressed. E-mail: macrae.1@nd.edu; fax: 219-631-8068.

10.1021/jp004170+ CCC: $20.00
Published on Web 03/13/2001

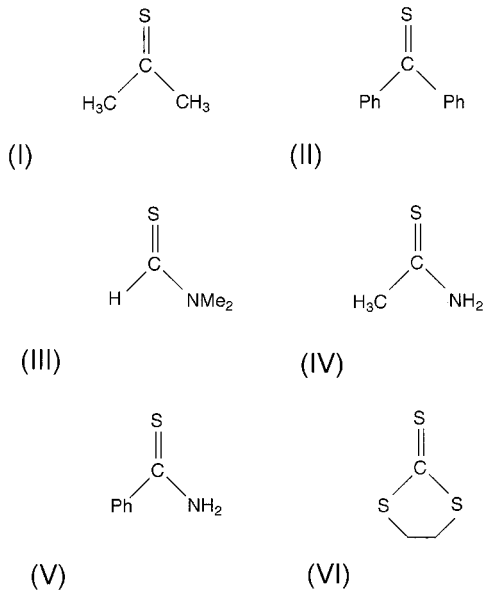

Figure 1. The six parent molecules to which H addition was considered.

tionals such as the MPW1−PW91 method of Adamo and Barone have been developed,[18] but there is evidence that results obtained using this method are effectively identical to those from B3LYP.[16]

The computations were performed using a parallel version of Gaussian 98[19] running on Silicon Graphics machines at Notre Dame. The basis set used was 6-311++G** throughout, which contains polarization and diffuse functions on all atoms and should be sufficiently flexible over both core and valence regions to yield reasonably accurate coupling constants for H, C, and N. For sulfur it is equivalent to the "negative-ion" version of the (621111,52111) McLean−Chandler basis set employed in calculations on SMu.[8] Basis sets (known as EPR-II and EPR-III) exist which are specifically adapted to the calculation of hyperfine properties;[20] however, these are limited to first-row atoms and are not appropriate here. In all cases, geometries were fully optimized at the B3LYP/6-311++G** level using analytical gradients and the Berny algorithm in redundant internal coordinates[21] and without symmetry. Initial geometries for the radicals were obtained using the CORINA/CACTVS system of Gasteiger et al.[22,23] Where difficulties were encountered with starting geometries, pre-optimizations were first carried out using the 6-31G basis set. The geometries were confirmed to be minima by the calculation of vibrational frequencies. The standard convergence criteria for energy, integrals, and geometry were adopted in geometry optimizations, while "tight" SCF convergence was enforced in single-point calculations.

3. Results and Discussion

Proton (Muon) Couplings. Figure 1 shows the set of parent compounds considered in these calculations. These are (**I**) dimethyl and (**II**) diphenyl thioketones, (**III**) *N*,*N*-dimethylthioformamide, (**IV**) thioacetamide, (**V**) thiobenzamide, and (**VI**) ethylene trithiocarbonate. The oxygen analogue of (**I**), acetone, was also considered for comparison.

The results of H(Mu) addition to these six molecules is considered in Table 1, where the first two columns give the calculated Fermi contact hyperfine coupling

$$A_{\mathrm{p}} = \frac{8\pi}{3} g_{\mathrm{e}} \beta_{\mathrm{e}} g_{\mathrm{H}} \beta_{\mathrm{N}} |\Psi(\mathbf{r_H})|^2 \qquad (2)$$

TABLE 1: Calculated Proton Couplings for C and S Adducts of I−VI with Relative Stabilities and Experimental Reduced Muon Couplings Where Available[a]

molecule	A_{p} (C adduct)	A_{p} (S adduct)	ΔE	A'_{μ} (expt)[b]
I	92.8	4.16	32	
II	24.2	14.1	−21	22[e]
III	61.7	145.0	29	154[e], 136[d]
IV	−0.06	137.3	27	153[a], 146[b], 137[c], 122[d]
V	−0.9	55.6	−16	63[a], 62[b], 57[c]
VI	0.37	123.0	22	108[a], 112[b], 109[c]

[a] Couplings are in MHz, stabilities in kJ mol^{-1} (with the energies corresponding to greater stability of the C adduct). Experimental couplings are room temperature values. [b] The data denoted with superscripts a, b, and c are in THF, EtOH, and formamide, respectively and come from ref. 12, while those marked d are in aqueous solution and come from ref 4. Data marked e come from ref 2.

for the optimized geometries of the C and S adducts. The next column gives ΔE, the isomeric energy difference (with $\Delta E > 0$ corresponding to a more stable C adduct), and the rightmost column gives the experimentally observed muon-electron hyperfine coupling constant A'_{μ}. ($A'_{\mu} \equiv A_{\mu} \cdot (\mu_{\mathrm{p}}/\mu_{\mu})$ is known as the *reduced* coupling and is directly comparable to proton couplings, with remaining differences being attributable to isotopic variation in dynamical conformational averaging. The current best value of $(\mu_{\mathrm{p}}/\mu_{\mu})$ is given in ref 24.) What is immediately apparent is that there is no clear division between "large" couplings for C adducts and "small" couplings for S adducts to support the conventional intuitive arguments;[2] indeed, in the majority of cases considered, the S adduct gives the larger coupling. This is straightforwardly rationalized in terms of the Heller−McConnell relation for β-couplings[25]

$$A_{\mu}(\gamma) = A + B \cos^2 \gamma \qquad (3)$$

in which γ is the dihedral angle measured from the position in which (in a model with a planar radical center − in fact, in hydroxyalkyls, for example, the radical center is well-known to be somewhat pyramidal[26−28]) the S-H (S-Mu) bond eclipses the projection of the $2p_x$ orbital on C in which the unpaired electron largely resides, and A and B are empirical parameters sometimes associated with spin-polarization and hyperconjugation, respectively. Arguments in favor of small couplings for S adducts are made by extension from the known couplings of hydroxyalkyl radicals, in which the energy minimum geometry usually has O-H lying in or near the $2p_x$ orbital's nodal plane [i.e., $\gamma_{\mathrm{min}} \sim (\pi/2)$]. Indeed, this is true also of the alkanethiol radicals derived from thioketones (adducts to **I** and **II**), and the couplings A_{p} are small as expected. However, in the presence of other functional groups the SH bond shows very different conformational behavior. In the adducts to **IV** and **VI**, $\gamma_{\mathrm{min}} \sim 0$, while in that to **V** it is about $(\pi/6)$, accounting for the large values of A_{p} calculated in these species. The wide variation in A_{p} values encountered in the S-centered (C-adduct) radicals is more difficult to account for. In all cases, the C center is tetrahedral and the spin density is nominally localized on the S atom. These radicals are structurally similar to the sulfanyl radical, SH, calculations on which are problematized by the degeneracy between the $2\pi_x^2 2\pi_y^1$ and $2\pi_y^2 2\pi_x^1$ configurations; this degeneracy is broken by replacement of H with CR_1R_2H, leading to an unpaired electron in a sulfur 3p orbital with some fixed geometrical relationship to the CH bond. The exact nature of the relationship, however, is subtly dependent on the character of the groups R_1 and R_2, which determine the extent and nature of the degeneracy-breaking. This can be formalized in terms of a rotation angle γ of the 2π orbital (or sulfur 3p orbital) with

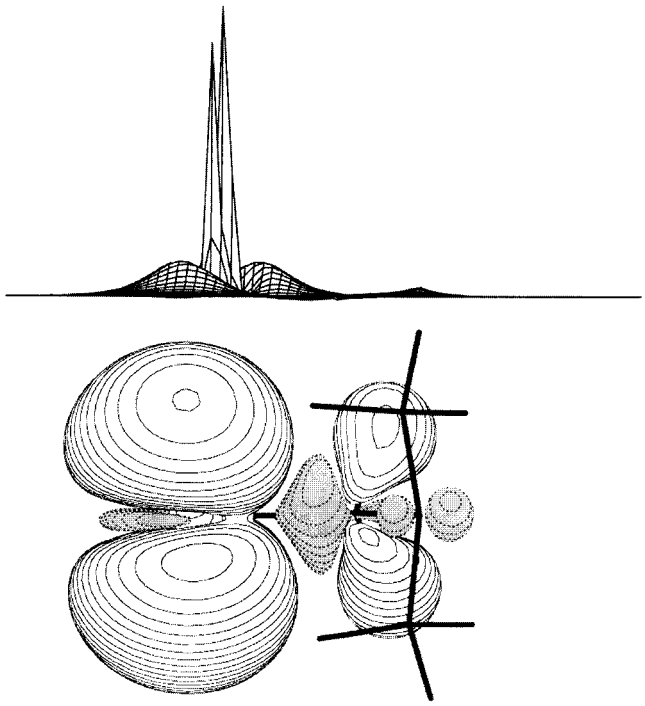

Figure 2. Spin density distribution in the C adduct of **III**. The upper figure shows the density in the CHS plane. The lower figure shows the three-dimensional density distribution (0.001 contour), with the symmetry axis perpendicular to the plane of the paper. The dihedral angle between the sulfur *p*-lobe axis and the C-H bond is about 30°.

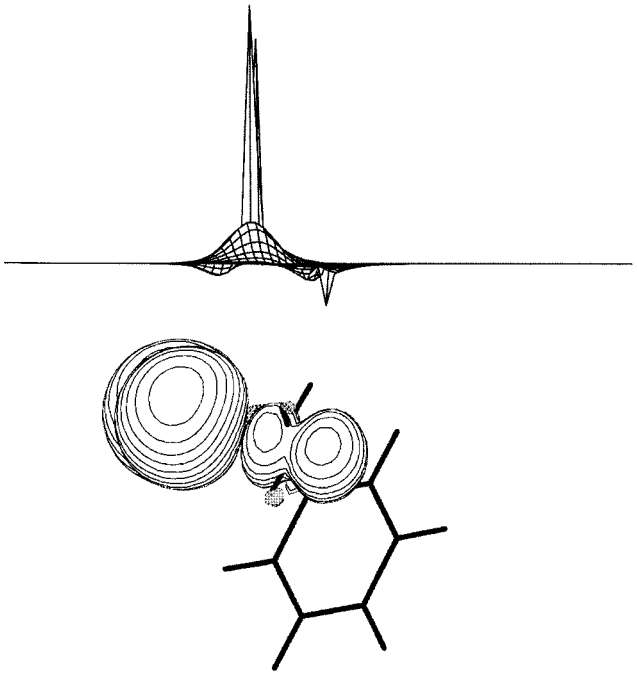

Figure 3. Spin density distribution in the C adduct of **V**. The upper figure shows the density in the CHS plane. The small negative spike is the spin density at C, and the density at H is essentially zero. The lower figure shows the three-dimensional density distribution (0.001 contour), with the CHS plane in the plane of the paper. The dihedral angle between the sulfur *p*-lobe axis and the C-H bond is about 70°.

respect to the C-H bond projection. (It is on the basis of this sort of picture that Rhodes et al. employ Heller−McConnell-like arguments in the discussion of thiyl radicals.[2]) That is,

$$\psi_\gamma(2\pi) = \cos\gamma\psi_x(2\pi) + \sin\gamma\psi_y(2\pi) \qquad (4)$$

where the *x* axis is identified with the C-H bond projection. Additionally, it may be that this angle γ is coupled to some large amplitude motion such as a torsion in R_1 or R_2; this would be the most likely mechanism for a significant temperature-dependence in the coupling constant. The issue of large amplitude motions and temperature dependences is discussed further below.

Comparing the computed values with the experimental A'_μ, it is clear that the S-adduct (C-centered) radicals give reasonable agreement in every case, while the C-adduct radicals deviate very strongly from experiment in cases **III**, **IV**, **V**, and **VI**.

The spin density distributions corresponding to the optimized geometries of the C atom adducts of **III** and **V** are shown in Figures 2 and 3. These are systems exhibiting fairly large (61.7 MHz) and small (−0.9 MHz) values of A_p, respectively, despite considerable structural similarities. The couplings seem reasonable in the light of the dihedral angles γ_{min} between the lobes of the sulfur p density and the C-H bond projection, $\gamma_{min} \sim 30°$ in the *N*,*N*-dimethyl thioformamide thiyl radical, while in the thiobenzamide thiyl radical $\gamma_{min} \sim 70°$. The difference in conformational preference arises most likely because in **III**, a tertiary thioamide, the dominating repulsions involve the methyl groups which are absent in **V**, a primary thioamide. Additionally, in **III**, the added H atom is symmetry-equivalent to that already attached to C. It may also be significant that the major part of the sulfur spin density comes from 3p atomic orbitals containing a radial node, which might be expected to have overlap behavior different from the 2p orbitals occupied in alkoxy radicals. Note in any case, though, that it is insufficient to consider only the structure of the α-HOMO,[12] as in these spin-unrestricted calculations the spatial mismatch between the uppermost occupied α-spin and β-spin orbitals is considerable, and several orbitals contribute to the spin density distribution; in both the cases illustrated, the p-lobe in the α-HOMO has a quite different orientation.

Degeneracy effects may be important in the C-atom adducts of **I** and **II**, particularly in **I** where the relatively facile methyl torsion will perturb the C_s symmetry of the system and lead to fluctuations in γ. (In **II**, steric interference between the two phenyl groups is significant; the optimum geometry has no reflection symmetry, and the phenyl torsions will be strongly coupled, with a substantial potential barrier separating the minima.)

Couplings at Other Nuclei. One of the advantages of the technique of avoided level-crossing muon spin resonance (ALC-μSR)[29,30] is that under favorable conditions the couplings of all nuclei in the radical with nonzero magnetic moments can be obtained simultanously, *together with their signs*. Measurements of this kind were carried out by Barnabas and Walker on aqueous solutions of **III** and **IV**, yielding ^{14}N and ^{1}H coupling constants.[4] The muon coupling constants corresponding to these (but actually obtained by the transverse field μSR technique) are shown (in their reduced form A'_μ) in the rightmost column of Table 1, denoted *d*). It is worthy of note that they are in each case smaller than those measured by Rhodes et al.,[11] probably indicating that the radicals are fairly strongly dipolar and interact considerably with water. The calculated values of $A(X)$ for all nuclei X showing substantial couplings in adducts of **III** and **IV** are presented in Table 2, together with the experimental values for $A(^1H)$ and $A(^{14}N)$.

Since the H atom lacks separate core and valence spaces, calculation of the on-site contribution to A_p (that is, the contribution from basis functions centered on H itself) is relatively straightforward; complications arise largely through behavior related to mechanisms of transmission of spin density through the molecular framework (spin polarization, hypercon-

TABLE 2: Fermi Contact Couplings of ^{1}H, ^{13}C, ^{14}N, and ^{33}S for C and S Adducts of III and IV (in MHz), Together with Experimental Values of ^{1}H and ^{14}N Couplings (Room Temperature Values, in Aqueous Solution) from Ref 4[a]

parent molecule	X	$A(X)$ (C adduct)	$A(X)$ (S adduct)	$A(X)$ (expt)
III	^{13}C (C-S)	−12.6	86.2	
	^{13}C (CH_3) (1)	−0.36	7.45	
	^{13}C (CH_3) (2)	−0.36	−3.75	
	^{33}S	6.95	61.9	
	^{14}N	−1.10	13.9	28.8
	^{1}H (C-H)	61.7	−35.4	61.4
	^{1}H (CH_3) (1)	(1.5, −0.2, −0.2) (0.37)	(4.2, 5.8, 24.2) (11.4)	
	^{1}H (CH_3) (2)	(1.5, −0.2, −0.2) (0.37)	(3.2, 5.1, 29.5) (12.6)	
IV	^{13}C (C-S)	−17.9	118.1	
	^{13}C (CH_3)	−1.7	−11.5	
	^{33}S	6.41	59.1	
	^{14}N	−0.55	9.53	24.7
	^{1}H (CH_3)	(1.62, −0.59, 2.14) (1.06)	(94.5, 22.2, 16.9) (44.5)	52.4
	^{1}H (NH_2)	(−6.62, −7.84) (−7.23)	(6.1, 7.0) (6.55)	

[a] Calculated methyl proton couplings are listed together with their arithmetic mean.

jugation, and so forth). While this leads to problems in UHF, for example, high-spin solutions contaminate the wave function, and couplings tend to be overestimated,[31] density functional methods seem remarkably well-behaved in this regard. (The correlation effects implicit in the technique are sufficient to remove nearly all spin contamination in most cases.) In first-row atoms, on the other hand, the presence of core and valence electrons leads to a situation in which the Fermi contact interaction is partly determined by two large on-site contributions of opposite sign;[31] even a small core polarization contribution can lead to a large shift in the coupling constant. While, subject to certain apparent systematic discrepancies, density functional theory gives reasonable results for many isolated first-row atoms and small molecules,[32] the above caveat should be borne in mind. For second-row atoms such as S, the situation is complicated still further due to the presence of another electronic shell, and the values presented here should not be regarded as even a qualitative attempt to calculate $A(^{33}S)$.

Thioacetamide, **IV**, is the simpler case and will be considered first. The resonances observed in ALC-μSR measurements on **IV** were interpreted by Barnabas and Walker as $\Delta M = 1$ resonances due to one or more protons (with $A_p = 61.4$ MHz) and the nitrogen nucleus (with $A(^{14}N) = 28.8$ MHz). While $A(^{14}N)$ seems rather large, this appears to be a reasonable interpretation, as the alternatives would imply either an unreasonably large A_p ($\sim$131 MHz) or an unphysical large negative $A(^{14}N)$ (~ -90 MHz). (In fact, the $I = 1$ ^{14}N nucleus gives rise to a doublet, with a splitting

$$\delta = \frac{A(^{14}N)^2}{\gamma_e(A_\mu - A(^{14}N))} \qquad (5)$$

amounting in this case to about 6×10^{-5} T, about 100 times smaller than the experimental line width.) Scanning the appropriate column of Table 2, it is evident that the C adduct (in which the unpaired spin is localized on S) does not allow either ^{1}H or ^{14}N couplings of such large magnitude, as relatively little spin can be transmitted through the molecular framework by spin polarization, hyperconjugation, or delocalization. In the S adduct, however, the center of spin density is the central C atom, and more possibilities for the transmission of spin density exist. In particular, the ^{14}N coupling is in reasonable agreement with experiment given the approximation, while the methyl protons clearly carry sufficient spin density that an averaged $A_p[CH_3]$ of 52.4 MHz is possible. If the methyl group has exact 3-fold symmetry and the Heller-McConnell relationship (eq 3) is exactly obeyed, it is simple to demonstrate that the arithmetic mean of the couplings is equal to the high-temperature average $A + (B/2)$ for *any* value of γ_0 (where γ_0 is the dihedral angle between one of the three C-H bonds and the *p*-orbital axis); this figure is given in the table together with the couplings. Again, if eq 3 is obeyed,

$$\gamma_0 = \frac{1}{2}\tan^{-1}\left\{\frac{\sqrt{3}[A_p(H_2) - A_p(H_3)]}{2A_p(H_1) - A_p(H_2) - A_p(H_3)}\right\} \qquad (6)$$

and the parameters A and B can be obtained trivially, by substitution and elimination. In this case, $A = -5.527$ MHz, $B = 100.12$ MHz, and $\gamma_0 = 1.75°$. The deviation between the calculated and the experimental values may imply that torsional averaging is incomplete. Note, however, that an additional potential source of error exists within the experiment: the ALC measurements were carried out under conditions of much greater dilution than the TF. Any variation in A_μ due to the concentration change (and it is clear from a comparison of Rhodes's and Walker's results that the solvation environment does affect A_μ) or to uncontrolled temperature variation will lead to an inaccurate interpretation of the $\Delta M = 0$ signals to extract hyperfine couplings $A(X)$. If the true A_μ in this system is, say, 5 MHz smaller than Barnabas and Walker assume, downward corrections of approximately equal size should also be made to $A(^{14}N)$ and A_p, bringing A_p into better agreement with the computed value. (In the solid state, it is often possible to observe the $\Delta M = 1$ line which unequivocally gives the correct A_μ under the conditions of the experiment, but rapid reorientation in the liquid averages to zero the hyperfine tensor components responsible for this transition. Alternatively, it may be possible to observe the signal under the same conditions as in the ALC measurements by employing the new "zero-frequency" technique of Schüth et al.[33])

The case of **III**, however, is more problematic. Alhough the reduced muon coupling, A'_μ, is in excellent agreement with the computed value for the S adduct, the other observed signals cannot straightforwardly be assigned given the computed couplings shown in the table. While the discrepancy in the ^{14}N coupling could conceivably be the result of basis set and conformational effects, it is not possible for any proton in this structure to have $A_p = 61.4$ MHz. (Basis set effects were checked for this system by comparing single-point calculations using 6-311++G** with those using EPR-II for all atoms except S, and 6-311++G** for S alone. The effect was minor for most nuclei, with ^{14}N showing the greatest effect, an increase of around 24%.) That the α-proton yields $A_p < 0$ is in line with analogous systems and a simple theoretical picture of spin polarization, while insufficient spin density is delocalized onto the methyl protons to yield such a large coupling. The situation is complicated slightly by the fact that the second minimum in the C-S torsional coordinate has an energy only 1kJ mol^{-1} higher than the global minimum, and yields A_p (A'_μ) = 99.4 MHz, the other couplings being similar to those tabulated, with the exception of that for ^{33}S, which is −3.07 MHz. (These and other conformational problems are discussed further below.) However, the explanation of the anomaly does not seem to lie in this direction. While it happens that the computed $A_p(CH_2)$ for the C adduct agrees almost exactly with the experimental A_p, it must be remembered that this value depends on an experimental A'_μ of 136 MHz. Such a deviation in couplings between a symmetry-equivalent (up to differences induced by zero-point stretching)

proton and muon is unprecedented. For methylenic protons in cyclohexadienyl-type radicals, it is usually assumed that $A'_\mu(\text{exp}) \sim 1.2A_p(\text{calc})$ and $A_p(\text{exp}) \sim 0.96\ A_p(\text{calc})$, in the ideal case.[34] In this case, the capacity of the lobes of unpaired spin density to rotate around the C-S bond generates an additional degree of freedom, which has the potential to generate qualitative (i.e., symmetry-breaking) and drastic changes in the electronic distribution. In the optimized C_s structure, $r_{CH}(CH_2) = 1.094$ Å. Zero-point effects will be dealt with more thoroughly in the following section, but as a simple estimate of their magnitude in this case, a calculation was performed in which one of the pair of C-H bonds was extended by 3%, a realistic zero-point stretch for C-Mu, and the structure allowed to reoptimize. (In the case of a true zero-point stretch, for a reasonable approximation the hyperfine coupling must be integrated over the full range of r for which the one-dimensional anharmonic ground-state vibrational wave function $|0\rangle$ has a significant value; this is likely to enhance the isotope effect.) For the initial stretched geometry, the results were A_p (long) = 65.3 MHz, A_p (short) 60.8 MHz, while after optimization the couplings were A_p (long) = 68.2 MHz, A_p (short) = 59.8 MHz. At this level of differential stretching, there is no evidence for dramatic changes in electronic structure, and it is therefore unlikely that A'_μ and A_p in the geminal pair can have such disparate values as would be implied by this interpretation of Barnabas and Walker's results.

It is noteworthy that the best agreement between theory and experiment for A'_μ (Table 1) is usually found with the experimental data of Rhodes et al., obtained in nonaqueous solvents. Clearly hydrogen-bonding is important in these systems, as it is for example in α-muoxyalkyl radicals formed by Mu addition to carbonyls;[35,36] this might be interpreted as an argument in favor of S as the addition site. The overall dipole moments μ_{tot} are larger in the S adducts to **III**, **IV**, and **VI**, and in the C adducts to **I**, **II**, and **IV**. While a full study of solvation effects is beyond the scope of this article, to obtain an impression of the magnitude of hydrogen-bonding effects on radical structures and hyperfine couplings, geometry optimizations were carried out on the C and S adducts of **IV** in the presence of one or two explicit H_2O molecules. The first water molecule predictably H-bonds to the amine lone pair in both the C and the S adduct, with little or no effect upon the proton hyperfine coupling in either case. In the S adduct, addition of a second H_2O molecule leads to a structure in which the new water molecule is H-bonded simultaneously to the proton of the thiol group via its oxygen atom and to the other water molecule via one of its protons. With the radical unrelaxed (i.e., at the optimum geometry obtained in the absence of water), this leads to a reduction of about 8 MHz in A_p. Relaxation of the overall system by full geometry optimization leads to a small diminution in the change in coupling. In the C adduct, a second H_2O molecule H-bonds rather more weakly to the S atom, and in this instance dependent on the geometry of the H-bonded complex (which in turn will be dependent on dynamical effects and the number of water molecules instantaneously associated with the radical) there can be substantial effects on the β-proton coupling. While this is unlikely to be the origin of effects experimentally observed (as the high couplings persist even in the absence of hydrogen-bonding solvents), it seems meritorious of further investigation.

The ΔE values given in Table 1 yield a relative stability series of (ordered corresponding to S adduct stability) **II** > **V** > **VI** > **IV** > **III** > **I**, with only **II** and **V** yielding a net thermodynamic preference for S addition. The radical formation process, however, is likely to be direct H (Mu) atom addition:[4] in the case of attack at C, this implies a transition state in which the system is strongly distorted from the reactant's initial geometry, while attack at S involves less such distortion. For the purpose of comparison, calculations were also carried out on the adducts of the O analogue of **I**, i.e., propan-2-one. Experimentally, this is known to yield addition at O.[37] In this case, addition at O is energetically preferred by 45 kJ mol^{-1}, and the relevant proton hyperfine couplings are 815 and −18 MHz for addition at C and O, respectively. (The very large size of A'_μ in the C adduct would probably preclude observation of this radical in conventional TFμSR experiments even if it were formed.)

Zero-Point Effects. The small mass of the muon (206.77 m_e[24]) results in large zero-point displacements in modes involving Mu; this necessitates corrections to the calculated frozen-geometry properties by integration over these coordinates. In what follows, we consider only the bond stretch; this coordinate is shown by consideration of harmonic frequency decompositions using the method of Boatz and Gordon[38] to be "vibrationally isolated",[39] and it is thus reasonable to treat it on its own. Since the muon's trajectory samples a large region of the potential, perturbative methods such as that introduced recently by Åstrand et al.[40] may not be appropriate; at the same time, use of an approximate exactly solvable potential such as the well-known one of Morse[41] may lead to inaccuracies in the fitting of r_e and the determination of $\langle 0|\delta r|0\rangle$ (where $\delta r = r - r_e$). Despite the popularity of the Morse potential, it is known to be a comparatively poor approximation to the experimental Rydberg−Klein−Rees potentials for diatomics.[42] An alternative approach for polyatomics is the Simons−Parr−Finlan expansion[43] embodied in SURVIB,[44] used by Webster et al. in consideration of the muonium isotopologues of water;[45] in this case, such a treatment would involve too many coordinates. We choose therefore to pursue the four-parameter exactly solvable potential of Wei Hua,[46] actually a generalized version of the Rosen−Morse and Manning−Rosen potentials.[47] It has the form

$$U(r) = D_e\left\{\frac{1 - \exp[a(c-1)(r-r_e)]}{1 - c\exp[a(c-1)(r-r_e)]}\right\}^2,\ |c| < 1 \quad (7)$$

which reduces to the Morse potential when $c = 0$. The connection between the parameter c and the molecular constants α_e and $\omega_e x_e$ has been brought out by Kaur and Mahajan.[48] The solutions to eq 7 are

$$\psi_n = N_n|x|^{\rho_{0n}}(1-x)^{\rho_c+1/2}F(-n, 1+n+2\rho_{0n}+2\rho_c, 1+2\rho_{0n}; x) \quad (8)$$

where

$$x = c\exp[a(1-c)(r-r_e)] \quad (9)$$

$$\rho_c = \text{sgn}(c)\rho \quad (10)$$

$$\rho = \left[\frac{1}{4} + t^2\left(\frac{1}{c} - 1\right)^2\right]^{1/2} \quad (11)$$

$$t = (2\mu D_e)^{1/2}/(\hbar a(1-c)) \quad (12)$$

$$\rho_{0n} = \left[t^2\left(\frac{1}{c}-1\right) - \rho_c\left(n+\frac{1}{2}\right) - \frac{\left(n+\frac{1}{2}\right)^2}{2} - \frac{1}{8}\right]\Big/\left(\rho_c + n + \frac{1}{2}\right) \quad (13)$$

and $F(\alpha, \beta, \gamma; x)$ is a Jacobi polynomial. The normalization

TABLE 3: Parameters Extracted from Fitting of the C-Mu, O-Mu, and S-Mu Stretches of Adducts to I and Its O Analogue, Using the Potentials of Morse[41] and Wei[46]

radical (bond)	r_e^G	r_e^M	r_e^W	$\langle dr^W\rangle_0$	$\langle A'_\mu\rangle_0$	c
Me_2CHS (C−H)	1.1003	1.1096	1.1005	00534	106.7	0.091
Me_2CSH (S−H)	1.3493	1.3283	1.3459	0.0493	7.88	−0.282
Me_2CHO (C−H)	1.1149	1.1102	1.1143	0.0588	293.6	−0.010
Me_2COH (O−H)	0.9631	0.9524	0.9637	0.0451	−4.04	−0.260

constant is given by

$$N_n = N_0^{\pm}\left(\frac{a(1-c)(2\rho_c+n+1+2\rho_{0n})(2\rho_{0n}+1)_n}{n!(2\rho_c+2n+1)B(2\rho_c+n+1,2\rho_{0n})}\right)^{1/2} \quad (14)$$

where

$$N_0^{+} = 1 \text{ for } c > 0 \quad (15)$$

$$N_0^{-} = \left\{\frac{\sin[(2\rho_{0n}+2\rho_c)\pi]}{\sin(2\rho_c)\pi}\right\}^{1/2} \text{ for } c < 0 \quad (16)$$

$B(\alpha, \beta)$ is the Beta function, and $(\alpha)_n$ is Pochhammer's symbol. The matrix elements are

$$\langle i|(r-r_e)^k|j\rangle = [a(1-c)]^{(k+1)}\int_{x_0}^{0} x^{-1}\left[\ln\left(\frac{x}{c}\right)\right]^k \psi_i(x)\psi_j(x)dx \quad (17)$$

where $x_0 = c\exp[a(1-c)r_e]$, and in this case the zero-point displacement $\langle\delta r\rangle_0$ is expressed as

$$\langle\delta r\rangle_0 = \langle 0|r-r_e|0\rangle \quad (18)$$

while the reduced hyperfine constant A'_μ has a corresponding corrected value given by expansion of the computed coupling A_p in powers of $(r - r_e)$, i.e.,

$$\langle A'_\mu\rangle_0 \equiv \langle 0|A'_\mu|0\rangle \quad (19)$$

$$= a_0 + \sum_{j=1}^{j_{max}} a_j\langle 0|(r-r_e)^j|0\rangle \quad (20)$$

A good fit is obtained with $j_{max} = 6$. The reduced muon mass $\mu = (m_\mu m_R/m_\mu + m_R)$, where m_R is the mass of the remaining part of the radical, differs from m_μ by only about 1 part in 1000 here. The calculations were carried out by computing 40 points over the range $0.75r_e^G \le r \le 1.75r_e^G$, where r_e^G is the value obtained at the energy minimum in a Gaussian 98 geometry optimization. (In the following, r_e^M and r_e^W will denote the values obtained by fitting the computed energies to the Morse and Wei potentials, respectively.) The fits were performed using the Levenberg−Marquardt technique as coded in *Mathematica*, and the matrix elements were calculated by numerical integration of eq 17. The accuracy of the numerical integration was verified by analytic calculation of the first six integrals.

A comparison of the Morse and Wei potentials for the computation of zero-point effects was carried out only for the C and S adducts of **I** and the C and O adducts of its oxygen analogue. The results are collected in Table 3. Not surprisingly, the agreement between r_e^W and r_e^G is consistently better than that between r_e^M and r_e^G, with the deviation between the latter two showing a correlation with $|c|$ (tabulated in the rightmost column); even in the worst case, however, the discrepancy in r_e is slightly smaller than the mesh size. Also correlated with c is $\langle\delta r^W\rangle_0 - \langle\delta r^M\rangle_0$ (only $\langle\delta r^M\rangle_0$ is tabulated), for $c < 0$ $\langle\delta r^M\rangle_0 - \langle\delta r^M\rangle_0 < 0$ while for $c > 0$ $\langle\delta r^M\rangle_0 - \langle\delta r^M\rangle_0 > 0$. The effect of these factors on $\langle A'_\mu\rangle_0$ is in fact very small, and the Morse fit yields values hardly differing from those obtained with Wei's potential. For large couplings, the shifts are around the 15% level, whereas for small couplings they are on the order of a few megahertz.

TABLE 4: Summary of Experimental Temperature Dependence Data[a]

		EtOH	$HCONH_2$	THF	DMTF
III	A'_μ(room T)	157	151	157	155
	dA'_μ/dT	−0.0858	−0.0851		−0.0641
IV	A'_μ(room T)	146	137	153	
	dA'_μ/dT	−0.1143	−0.1143	−0.1737	
V	A'_μ(room T)	62	57	63	
	dA'_μ/dT	+0.0213	−0.0056	+0.0160	
VI	A'_μ(room T)	112	109	108	
	dA'_μ/dT	−0.0839		−0.0622	

[a] Values lacking temperature-dependences are from ref 11; the others are from ref 12. Couplings are in MHz and gradients are in MHz/K.]

These results strengthen the conclusion that zero-point effects cannot lead to the kind of differences required to account for Walker's A'_μ and A_p data in **III**.

As a prelude to the averaging calculations described in the following section, zero-point corrections to A'_μ at the geometries of maximum and minimum coupling were also carried out for the S adducts of **III**, **IV**, and **V**, using only the Wei potential. While at the minimum coupling geometry the zero-point correction was found to be negligible (with an absolute value on the order of 1 MHz), the effect at the maximum coupling geometry was found to be rather large, respectively, 58.9, 56.7, and 39.9 MHz. This is a consequence of the fact that from this geometry there is a smooth transition to the broken-bond limit where the spin density is entirely located on the isolated H atom, and the vibrational excursions of Mu in the strongly anharmonic potential predominantly sample the $r > r_e$ region.

Thermal Effects and Averaging over Large Amplitude Modes. The experimental temperature dependences of A'_μ were obtained by Rhodes et al.[12] for radicals formed in **III**, **IV**, **V**, and **VI** in ethanol (**III**, **IV**, **V**, **VI**), formamide (**III**, **IV**, **V**), tetrahydrofuran (**IV**, **V**, **VI**), and *N*,*N*-dimethylformamide (**III**); these data are summarized in Table 4 in the form of A'_μ (room T) and dA'_μ/dT for each system. As noted above, the couplings all show solvent effects, with the largest values of A'_μ being found in most cases in the nonpolar ether THF, and all have negative temperature-dependences with the exception of that in **V**, which is virtually temperature-independent, with a dA'_μ/dT whose sign varies depending on the solvent (and an A'_μ which is substantially smaller than the others). Additionally, although no tabulated couplings were published, Brodovitch et al. studied the temperature-dependence in **VI** through the freezing transition;[13] at the freezing point, the coupling was observed to jump from $A'_\mu \sim 110$ MHz to $A'_\mu \sim 134$ MHz, with two similar but distinct species (in terms of their couplings) observable in the frozen phase.

A full theoretical treatment of dA'_μ/dT in these species is beyond the scope of this article, as several of the radicals are structurally complex, with the possibility of several large-amplitude modes contributing to the temperature-dependence. From a simple intuitive standpoint, however, it is clear that dA'_μ/dT in the S-adduct alkanethiol radicals is likely to originate mainly in torsions around the nominally single C-S bond, while in the thiyl radicals the temperature-dependence is contingent upon the relative orientation of the sulfur 3p orbital and the

C-Mu bond; conformational effects (e.g., from other torsions or from the inversion of amide groups) are less transparent. The experimental data do, however, contain puzzling features; it is difficult, for example, to see how a thiyl radical interpretation of the adduct to **VI** can yield a large amplitude motion likely to produce a dA'_μ/dT of the magnitude observed or strong intermolecular interactions which might lead to a freezing-point phenomenon of the type described by Brodovitch. (On the other hand, an alkanethiol interpretation of **VI** leads naturally to this sort of behavior via trapping of the radicals on freezing in one or the other minimum of an unsymmetrical but broadly 2-fold C-SMu torsional potential; in the present calculations, the overall torsional minimum gives a coupling of 123 MHz, while the secondary minimum gives a coupling of approximately 117 MHz.)

Given a one-mode interpretation of dA'_μ/dT, in the spirit of the Heller−McConnell expression (eq 3) A'_μ (now viewed as an operator) can be expressed as an expansion in the torsional angle γ as

$$A'_\mu(\gamma) = A_0 + \sum_{j=1}^{j_{max}} A_j \cos(\gamma - \gamma_{0j}) \tag{21}$$

allowing the individual contributions to have different phase factors reflecting their different conformational origins. The torsional potential is expressed in a similar fashion, as

$$V(\gamma) = \sum_{j=1}^{j_{max}} \frac{V_j}{2}(1 - \cos[j(\gamma - \gamma_{0j})]) \tag{22}$$

and solved in a basis of free internal rotation wave functions

$$\phi_n = (2\pi)^{(-1/2)} \exp(in\gamma),\ n = -n_{max}, -n_{max}+1, ..., n_{max}-1, n_{max} \tag{23}$$

to yield eigenfunctions

$$\psi_j = (2\pi)^{(-1/2)} \sum_{k=-n_{max}}^{n_{max}} c_{nj}\phi_n(j) \equiv |j\rangle \tag{24}$$

Noting the matrix element identities over the basis functions

$$\langle m|\cos j\gamma|m'\rangle = \begin{cases} 0, & m' \neq m \pm j \\ \pi, & m' = m \pm j \end{cases} \tag{25}$$

$$\langle m|\sin j\gamma|m'\rangle = \begin{cases} 0, & m' \neq m \pm j \\ \pm i\pi, & m' = m \pm j \end{cases} \tag{26}$$

the general terms in the expression for $\langle A'_\mu\rangle_i$

$$\langle i|\cos\{j(\gamma - \gamma_{0j})\}|i\rangle = \frac{1}{2\pi}\sum_{m,m'} c^*_{mi}c_{m'i}\langle m|\cos\{j(\gamma - \gamma_{0j})\}|m'\rangle \tag{27}$$

can be written

$$\sum_m \{\cos(j\gamma_{0j})R[c^*_{mi}c_{m+j,i}] + i\sin(j\gamma_{0j})I\ [c^*_{mi}c_{m+j,i}]\} \tag{28}$$

In more symmetric cases, where the torsional coordinate includes a point where the molecule contains a mirror plane, the potential function can be written using only even terms, and this expression can be simplified, by observing that the c_{mi} are now all real, to the following form:

$$\cos(j\gamma_{0j})\sum_m c_{mi}c_{m+j,i} \tag{29}$$

The temperature-dependent hyperfine coupling constant can then be calculated from

$$A'_\mu(T) = \frac{\sum_i \langle A'_\mu\rangle_i \exp(-E_i/kT)}{\sum_i \exp(-E_i/kT)} \tag{30}$$

The calculated potentials and γ-dependences of A_p (A'_μ) for the C-S torsion in the S-atom adducts to **III**, **IV**, and **V** are shown in Figures 4−6. The potential shown as a heavy curve is the result of a relaxed optimization and takes the global energy minimum geometry as its coordinate origin. Assuming that density functional theory gives an accurate representation of the potential elsewhere than at the equilibrium geometry (counterexamples are known in which simple density functional treatments lead to overestimation of torsional barriers[49]), this constitutes a lower bound on the true potential curve. A corresponding upper bound would then be given by a rigid torsion calculation. The two extremes treat the torsion respec-

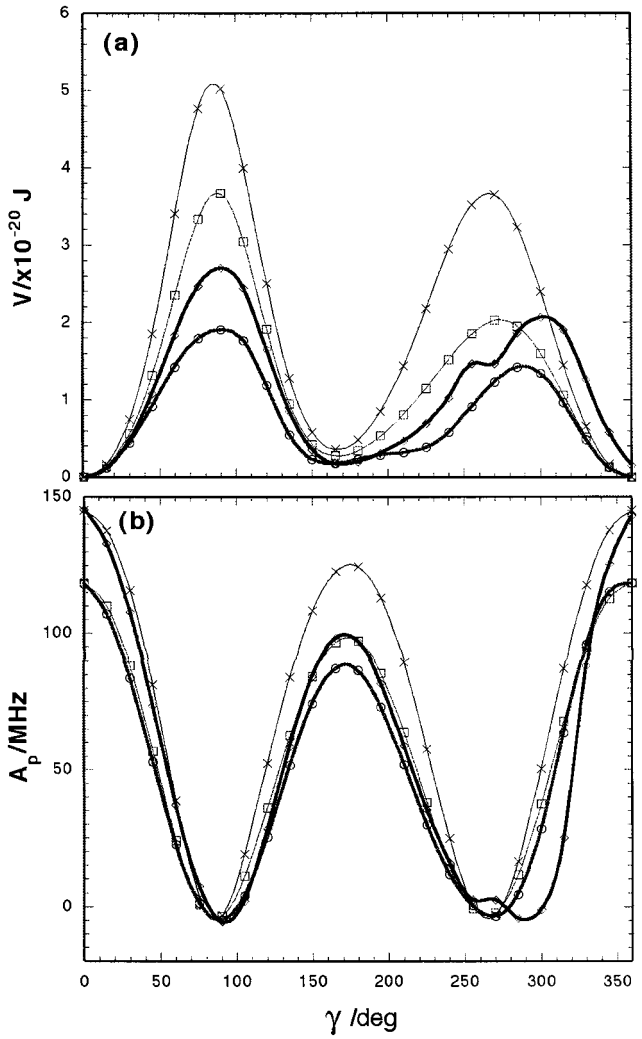

Figure 4. Relaxed and rigid C-S torsional potentials $V(\gamma)$ (a) and SH proton couplings $A_p(\gamma)$ (b) for the S adduct to *N*,*N*-dimethylformamide calculated using B3LYP and UHF. Key: circles: UHF, relaxed; squares: UHF, rigid; diamonds: B3LYP, relaxed; crosses: B3LYP, rigid.

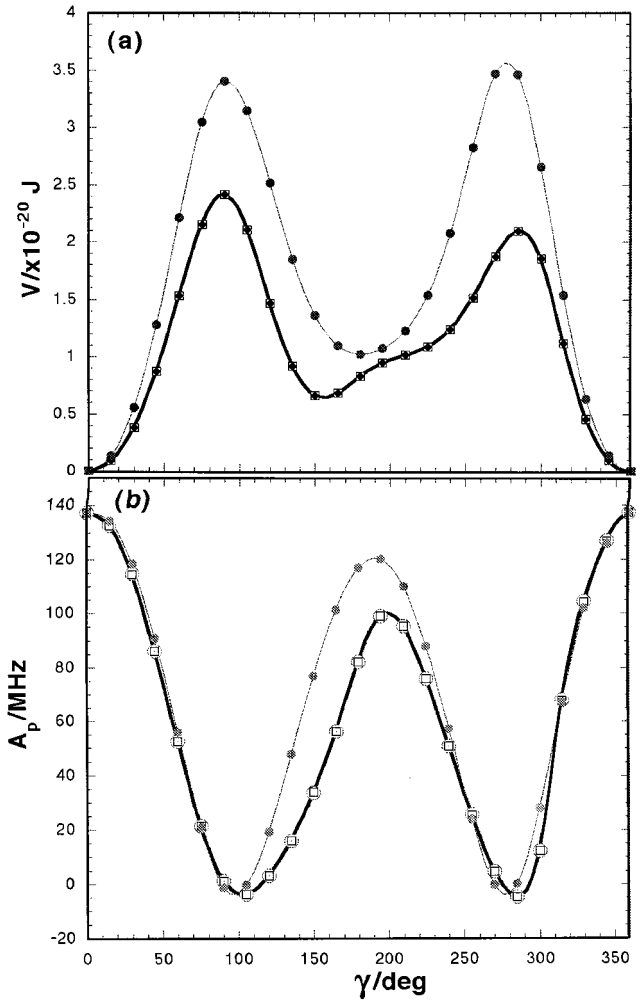

Figure 5. Relaxed (dark) and rigid (light) C-S torsional potentials $V(\gamma)$ (a) and SH proton coupling $A_p(\gamma)$ (b) for the S adduct to thioacetamide. The relaxed curves show the superposition of points obtained by the two methods described in the text.

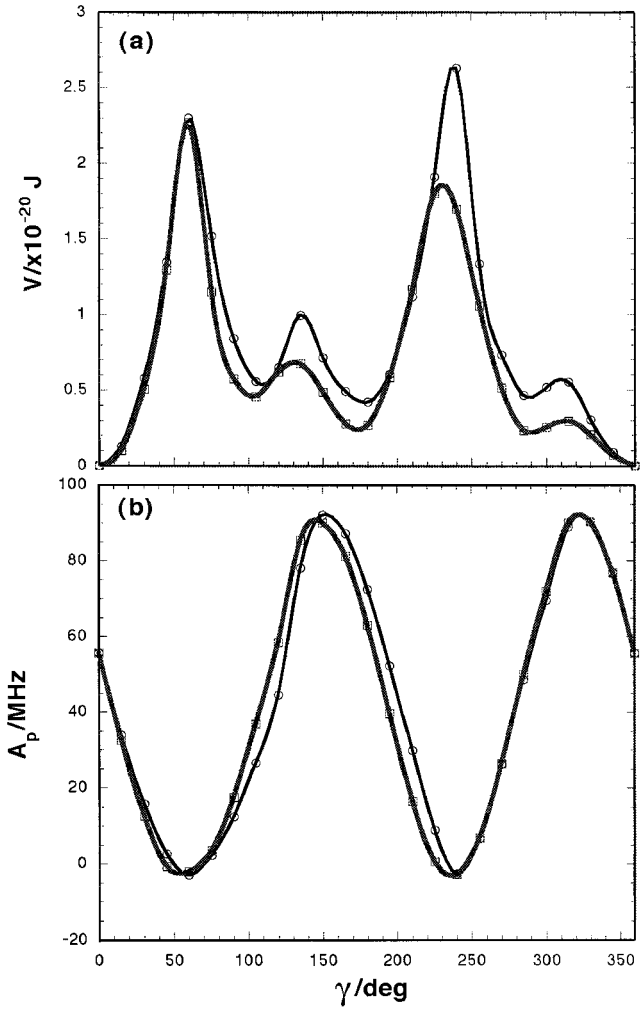

Figure 6. Relaxed C-S torsional potential $V(\gamma)$ (a) and SH proton coupling $A_p(\gamma)$ (b) for the S adduct to thiobenzamide. The curves represent the torsions defined with respect to angles CCSH (black, circles) and NCSH (grey, squares), respectively.

tively as an "adiabatic" and as a "tunnelling" mode. In cases where rigid torsions were performed, the results are shown on the same figure as a light curve.

The results of fitting the data plotted in these figures to eqs 21 and 22 are displayed in Table 5. It should be emphasized that the choice of fitting terms is somewhat arbitrary and need not reflect, for example, specific intergroup interactions. The fits were performed using the nonlinear Levenberg−Marquardt method as implemented in *Mathematica*. (Additionally, to check for method-dependences, selected relaxed optimizations were performed in two different ways. In the first, the built-in *scan* algorithm of Gaussian 98 was used, while in the second constrained optimizations were performed using externally generated starting geometries. In the case of radical **IV**, the points obtained using the two methods exactly overlie one another.)

It is immediately evident from the plots that the potential minima in **III** and **IV** lie near maxima in $A_p(\gamma)$, yielding high "frozen geometry" values of A_p and suggesting the likelihood that $dA_p/dT < 0$. In order to calculate theoretical values for $A_p|_{300K}$ and dA_p/dT, the reduced moments of inertia for internal rotation I_R are calculated according to

$$I_R = \frac{I_{top} I_{frame}}{I_{top} + I_{frame}} \tag{31}$$

where the moments I_{top} and I_{frame} are calculated with respect to the C-S internuclear axis. In the case of relaxed internal rotation (i.e., coupled modes), this value is not a constant. Although new methods exist which are capable of treating this phenomenon,[50] we note that its influence is smaller than 1% (and considerably less, for example, than the difference between values from UHF and B3LYP equilibrium conformations) and use the $\gamma = 0$ value for all geometries. The values used for **III**, **IV**, and **V** were 0.3396, 0.3428, and 0.3391 ($\times 10^{-47}$ kg m^2), respectively. As has been noted previously in work on Mu adducts to C═O,[51] in these systems (where in frame-fixed coordinates only H(Mu) is in motion) the light atom term almost completely determines I_R, and therefore the variation within a congeneric group (C═O adducts, C═S adducts) is very small. Another point worthy of note is that the low symmetry of these systems does not allow the torsional angle to be uniquely defined. In **V**, for example, runs were carried out taking 15° steps in ∠CCSH and ∠NCSH, respectively; the results, shown in Figure 6, indicate that these two coordinates interact slightly differently with out-of-plane deformations at the radical center. Considerations of this kind can under certain circumstances invalidate the notion of a "relaxed" torsional coordinate completely, if, for example, the trajectory through the torsion-inversion phase space contains bifurcations, hysteresis loops, or catastrophes.[52]

TABLE 5: Parameters Extracted from Fitting of the C-S Torsional Potentials for the S Adducts of III, IV, and V to eq 22[a]

system	n	V_n	γ^V_{0n}	A_n	γ^A_{0n}
	0			53.9797 (71.6596)	
	1	−0.55327 (0.42484)	38.72 (−58.71)	17.5392 (10.1934)	36.80 (21.12)
	2	2.05041 (3.96297)	6.21 (−4.84)	62.4075 (68.5462)	1.68 (−3.68)
III	3	0.80449 (0.62308)	259.40 (262.47)	−13.1106 (3.2262)	195.32 (21.05)
	4	−0.04280 (−0.74574)	−64.65 (266.28)	6.2433 (−6.5668)	−279.27 (173.47)
	5				
	6	0.03343 (−0.23103)	−76.77 (−94.74)	−2.1522 (−1.13704)	−230.46 (−216.61)
	0			58.01 (68.408)	
	1	0.42149 (0.68658)	−11.65 (1.41)	24.3477 (9.36615)	−15.46 (−18.41)
	2	1.75121 (2.89632)	1.24 (3.19)	58.5904 (65.3110)	11.12 (7.39)
	3	0.58776 (0.41699)	251.02 (−1.24)	−10.6919 (−3.46528)	−317.42 (−196.88)
IV	4	−0.35976 (−0.48884)	−349.97 (−264.01)	2.7769 (−5.74473)	−215.25 (−83.48)
	5	−0.12660	−133.69	−3.9743 (−1.10678)	7.79 (0.36)
	6	−0.03631 (0.01907)	50.75 (130.25)	−2.4663 (1.06026)	349.61 (246.56)
	7	0.03676	−38.63		
	8	0.01039	4.36		
	0			41.6849	
	1	0.34608	−19.15	−3.6415	77.42
	2	1.18695	−30.18	46.3179	−32.68
	3	−0.24184	203.73	−3.3535	355.15
	4	0.80155	278.20	−2.2964	−76.64
V	5	−0.3023	206.14	0.6355	−3.79
	6	−0.34047	58.40	1.3298	20.59
	7	0.07320	−118.14		
	8	−0.21392	−211.78		
	9	0.05748	0.48		
	10	0.04275	40.32		

[a] Potential terms are in $\times 10^{-20}$ J, hyperfine terms are in megahertz, and angles are in degrees. Main values are from relaxed scans; values in parentheses are from rigid scans.

The temperature-dependent hyperfine coupling constant, $A_p(T)$, was calculated using the formalism given above. In general, $A_p(T)$ has asymptotic values of

$$A_p(T \rightarrow 0) = A_0 + \sum_{j=1}^{j_{max}} A_j \langle 1|\cos j(\gamma - \gamma_{0j})|1\rangle \qquad (32)$$

which corresponds to the frozen minimum value plus some zero-point correction (in the limit that this correction is zero the asymptote is $A_0 + \sum_{j+1}^{j_{max}} A_j \cos \gamma_{0j}$ for a potential with a single global minimum at $\gamma = 0$), and

$$A_p(T \rightarrow \infty) = A_0 \qquad (33)$$

corresponding to the classical averaging of all oscillatory terms to zero. The behavior between these two limits depends on I_R and the nature of $V(\gamma)$, but for typical systems the region in the vicinity of room temperature is roughly linear, and an approximate value of dA_p/dT can be extracted from this linear relationship. Using the temperature range 250−400 K, the following linear relations were obtained for **III**, **IV**, and **V** (CCSH torsion):

III: $A_p(T) = 100.585 - 0.0312\ T/K$ (relaxed)

III: $A_p(T) = 131.565 - 0.0260\ T/K$ (rigid)

IV: $A_p(T) = 125.928 - 0.0770\ T/K$ (relaxed)

IV: $A_p(T) = 131.030 - 0.0395\ T/K$ (rigid)

V: $A_p(T) = 64.548 - 0.0227\ T/K$ (relaxed)

To these values should be added some correction for zero-point effects on the associated bending and stretching coordinates. The bending coordinate is essentially ignored in the present treatment; in the relaxed scan it is treated adiabatically, but without averaging or zero-point correction. (Thanks to the small mass of the muon, angle-bending frequencies − or at least *intrinsic* frequencies[38] − are ∼ 3× conventional X_1X_2H frequencies; as this exceeds kT at ambient temperatures, only zero-point effects on bending need usually be considered. These effects will be given further consideration in a separate study on a simpler system.[53])

Since although the torsional potentials are somewhat complex the angle-dependence of A_p is considerably simpler, being in most cases dominated by a single 2-fold term in the Heller−McConnell manner, zero-point corrections were carried out in accordance with the results of the previous section by adding a 2-fold term to $A_p(\gamma)$ in phase with the leading term. It was assumed that corrections to $V(\gamma)$ were negligible by comparison. Note that in **III** and **IV** the maxima in A_p correspond to the minima in V, while in **V** A_p and V are out of phase, leading to a likely strong negative temperature-dependence (as observed) in the first two systems and a more ambiguous situation (as observed) in the third. Given these corrections the linear relations become:

III: $A_p(T) = 153.470 - 0.0484\ T/K$ (relaxed)

IV: $A_p(T) = 177.901 - 0.0987\ T/K$ (relaxed)

V: $A_p(T) = 94.618 - 0.0321\ T/K$ (relaxed)

which leads to A'_μ(300K) values of 139.0, 148.3, and 85.0 MHz, respectively. These, in particular **III** and **IV**, are in extremely good agreement with the experimental values, and in the case of **IV** most of the temperature-dependence is also recovered. The missing component is likely to originate in zero-point averaging over the HCN bend, neglected in the present treatment.

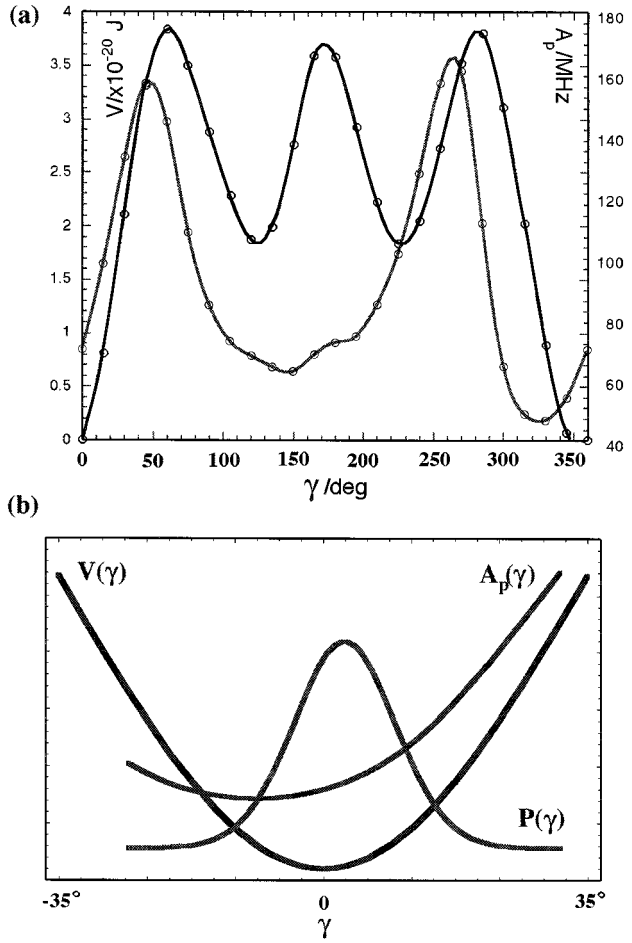

Figure 7. (a) Relaxed C-N torsional potential in the C adduct of *N*,*N*-dimethylformamide, additionally showing $A_p(\gamma)$ (for one of the two protons symmetry-equivalent at $\gamma = 0$); (b) region around $\gamma = 0$ used in the classical model, showing $V(\gamma)$, $A_p(\gamma)$, and $P(\gamma)$, the probability distribution for torsional excursions (defined in the text).

Only a limited attempt was made to study dA_p/dT in the C atom adducts. The great difference between the frozen values of A_p obtained in **IV** and **V** and the experimental values of A'_μ immediately implies that thermal averaging will not substantially improve matters. Closer attention was paid, however, to **III**, where the situation is more ambiguous. In this case, the main part of whatever temperature-dependence exists is likely to be due to torsion around the C-N bond. Calculations reveal that the orientation of the spin density lobe on the S atom does not depend strongly on this torsional angle. In this radical, I_R is determined predominantly by factors other than m_μ, and takes the value 147.2×10^{-47} kg m^2, almost 500 times larger than in the S adducts. Consequently, the torsional levels are much more closely spaced, zero-point effects are very small, and the quantized model used above requires a large expansion to yield convergence. The converged linear relationship given by the quantum model is

$$A_p(T) = 58.575 + 0.0226\ T/K$$

The temperature dependence is actually somewhat nonlinear over the fitting region leading to an underestimate of the "asymptote" and an overestimate of the gradient. Because I_R is large and the barrier is fairly high it may be supposed that a classical model will also give reasonable results. In this case, we consider only the region of the potential in the vicinity of the global minimum and use the approximation

$$A_p(T) = \frac{\int_{\gamma_0-\delta}^{\gamma_0+\delta} \exp(-V(\gamma)/kT) A_p(\gamma) d\gamma}{\int_{\gamma_0-\delta}^{\gamma_0+\delta} \exp(-V(\gamma)/kT) d\gamma} \quad (34)$$

The limits δ were chosen such that $P(\gamma) = \exp(-V(\gamma)/kT)$ at 300 K was entirely confined within the range $\gamma_0 - \delta < \gamma < \gamma_0 + \delta$. Using this method A_p(300 K) was calculated to be 64.34 MHz, with a temperature dependence of 0.00824 MHz/K. Figure 7 shows the relevant region of $V(\gamma)$, $A_p(\gamma)$, and $P(\gamma)$.

4. Conclusions

Calculations at the UB3LYP/6-311++G** level on the electronic structures of H adducts to the C and S atoms of a series of thioketones, thioamides, and thiocarbonates revealed that conformational influences from the amine and other functional groups invalidate simple models in which adducts to C are supposed to have large couplings while adducts to S have small couplings. The products of addition at C are energetically favored in most cases, but this factor may be overridden experimentally by the need to overcome a barrier to distortion at the C atom during the change in hybridization. Alternatively, if the formation mechanism is ionic, with initial electron attachment followed by μ^+ addition, the S addition position may be favored by factors related to charge distribution. The muon hyperfine couplings observed in TFμSR experiments by Rhodes et al.[2,12,13] are well accounted for by assuming all additions to be at S; the ALC-μ SR results of Barnabas and Walker[4] are more ambiguous, but there is some leeway for reinterpretation in the experimental data. Experiments on ^{13}C isotopically enriched samples or using the new "zero-frequency" resonance technique[33] might clarify matters. Zero-point corrections for bond stretching carried out using the potentials of Morse[41] and Wei[46] revealed that while Wei's potential yields superior zero-point corrections to r and a better fit to r_e, improvement in the zero-point correction to the hyperfine coupling is minor. Consideration of the angular dependence of the potential V and the coupling A_p reinforced the assignment of the observed signals to S adducts; thermal averaging performed over zero-point corrected relaxed torsional coordinates accurately reproduced the experimental couplings, but in the case of **III** and **V** recovered only part of the experimental temperature-dependence, probably due to inadequate treatment of averaging over bending coordinates.

Acknowledgment. The authors thank a reviewer of this paper for drawing their attention to ref 13. This work was supported by the Office of Basic Energy Sciences of the U. S. Department of Energy. This is contribution No. NDRL-4274 from the Notre Dame Radiation Laboratory.

References and Notes

(1) Roduner, E. *Radiat. Phys. Chem.* **1986**, *28*, 75.
(2) Rhodes, C. J.; Symons, M. C. R.; Roduner, E. *J. Chem. Soc. Chem. Commun.* **1988**, 3.
(3) Cox, S. F. J.; Symons, M. C. R. *Radiat. Phys. Chem.* **1986**, *27*, 53.
(4) Barnabas, M. V.; Walker, D. C. *Chem. Phys. Lett.* **1990**, *168*, 9.
(5) *S-Centered Radicals*, Z. B. Alfassi, Ed.; Wiley: New York, 1999.
(6) Kalyanaraman, B. *Biochem. Soc. Symp.* **1995**, *61*, 55.
(7) Halliwell, B.; Gutteridge, J. M. C. *Free Radicals in Biology and Medicine*; Clarendon Press: Oxford, 1989.
(8) Webster, B. C.; McCormack, K. L.; Macrae, R. M. *J. Chem. Soc., Faraday Trans.* **1997**, *93*, 3423.
(9) Curtiss, L. A.; Nobes, R. H.; Pople, J. A.; Radom, L. *J. Chem. Phys.* **1992**, *97*, 6766.
(10) Rauk, A.; Yu, D.; Armstrong, D. A. *J. Am. Chem. Soc.* **1998**, *120*, 8848.

(11) Rhodes, C. J.; Hinds, C. S.; Morris, H.; Reid, I. D. *Free. Rad Res.* **1997**, *27*, 347.
(12) Rhodes, C. J.; Dintinger, T. C.; Hinds, C. S.; Morris, H.; Reid, I. D. *Magn. Reson. Chem.* **2000**, *38*, S49.
(13) Brodovitch, J.-C.; Ji, F.; Percival, P. W.; Bischoff, A. L.; Pinto, B. M.; Addison-Jones, B.; Wlodek, S. *Hyp. Int.* **1994**, *87*, 839.
(14) Rhodes, C. J.; Symons, M. C. R. *Magn. Reson. Chem.* **1996**, *34*, 631.
(15) Engström, M.; Vahtras, O.; Ågren, H. *Chem. Phys. Lett.* **2000**, *328*, 483.
(16) Mattar, S. M. *Chem. Phys. Lett.* **1999**, *300*, 545.
(17) Becke, A. D. *J. Chem. Phys.* **1993**, *98*, 5648.
(18) Adamo, C.; Barone, V. *J. Chem. Phys.* **1998**, *108*, 664.
(19) *Gaussian 98* (Revision A.6), Frisch, M. J.; Trucks, G. W.; Schlegel, H. B.; Scuseria, G. E.; Robb, M. A.; Cheeseman, J. R.; Zakrzewski, V. G.; Montgomery, J. A., Jr.; Stratmann, R. E.; Burant, J. C.; Dapprich, S.; Millam, J. M.; Daniels, A. D.; Kudin, K. N.; Strain, M. C.; Farkas, O.; Tomasi, J.; Barone, V.; Cossi, M.; Cammi, R.; Mennucci, B.; Pomelli, C.; Adamo, C.; Clifford, S.; Ochterski, J.; Petersson, G. A.; Ayala, P. Y.; Cui, Q.; Morokuma, K.; Malick, D. K.; Rabuck, A. D.; Raghavachari, K.; Foresman, J. B.; Cioslowski, J.; Ortiz, J. V.; Stefanov, B. B.; Liu, G.; Liashenko, A.; Piskorz, P.; Komaromi, I.; Gomperts, R.; Martin, R. L.; Fox, D. J.; Keith, T.; Al-Laham, M. A.; Peng, C. Y.; Nanayakkara, A.; Gonzalez, C.; Challacombe, M.; Gill, P. M. W.; Johnson, B.; Chen, W.; Wong, M. W.; Andres, J. L.; Gonzalez, C.; Head-Gordon, M.; Replogle, E. S.; and Pople, J. A. Gaussian, Inc.: Pittsburgh, PA, 1998.
(20) Barone, V. In *Advances in Density Functional Methods*; D. P. Chong, Ed.; World Scientific: Singapore, 1995.
(21) Peng, C.; Ayala, P. Y.; Schlegel, H. B.; Frisch, M. J. *J. Comput. Chem.* **1996**, *17*, 49.
(22) Sadowski, J.; Gasteiger, J. *Chem. Rev.* **1993**, *93*, 2567.
(23) Ihlenfeldt, W. D.; Takahashi, Y.; Abe, H.; Sasaki, S. *J. Chem. Inf. Comput. Sci.* **1994**, *34*, 109.
(24) Mohr, P. J.; Taylor, B. N. *Rev. Mod. Phys.* **2000**, *72*, 351.
(25) Heller, C.; McConnell, H. M. *J. Chem. Phys.* **1960**, *32*, 1535.
(26) Solgadi, D.; Flament, J.-P. *Chem. Phys.* **1985**, *98*, 387.
(27) Cirelli, G.; Ha, T. K.; Meyer, R.; Gunthard, H. H. *Chem. Phys.* **1982**, *72*, 15.
(28) Macrae, R. M.; Webster, B. C.; Roduner, E. *IOP Short Meetings Series* **1990**, *22*, 95.
(29) Abragam, A. *C. R. Acad. Sci., Paris* **1984**, *299*, 95.
(30) Kiefl, R. F.; Kreitzman, S.; Celio, M.; Keitel, R.; Luke, G. M.; Brewer, J. H.; Noakes, D. R.; Percival, P. W.; Matsuzaki, T.; Nishiyama, K. *Phys. Rev. A* **1986**, *34*, 681.
(31) Chipman, D. M. *J. Chem. Phys.* **1983**, *78*, 4785.
(32) Carmichael, I. *J. Phys. Chem. A* **1997**, *101*, 4633; Kong, J.; Eriksson, L. A.; Boyd, R. J. *Chem. Phys. Lett.* **1994**, *217*, 24.
(33) Schüth, J.; Percival, P. W.; Addison-Jones, B.; Brodovitch, J.-C.; Ghandi, K. *Physica B* **2000**, *289*−*290*, 681.
(34) Percival, P. W.; Addison-Jones, B.; Brodovitch, J.-C.; Ghandi, K.; Schüth, J. *Can. J. Chem.* **1999**, *77*, 326.
(35) Hill, A.; Symons, M. C. R.; Cox, S. F. J.; de Renzi, R.; Scott, C. A.; Bucci, C.; Vecli, A. *J. Chem. Soc., Faraday Trans.* **1985**, *81*, 433.
(36) Buttar, D.; Macrae, R. M.; Webster, B. C.; Roduner, E. *Hyp. Int.* **1990**, *65*, 927.
(37) Hill, A.; Allen, G.; Stirling, G.; Symons, M. C. R. *J. Chem. Soc., Faraday Trans.* **1982**, *78*, 2959.
(38) Boatz, J. A.; Gordon, M. S. *J. Phys. Chem.* **1989**, *93*, 1819.
(39) Macrae, R. M. *KEK Proceedings 98-8, JHF-98-3*, **1998**, 81.
(40) Åstrand, P.-O.; Ruud, K.; Sundholm, D. *Theor. Chem. Acc.* **1999**, *103*, 365.
(41) Morse, P. M. *Phys. Rev.* **1929**, *34*, 57.
(42) Steele, D.; Lippincott, E. R.; Vanderslice, J. T. *Rev. Mod. Phys.* **1962**, *34*, 239; Levine, I. N. *J. Chem. Phys.* **1966**, *45*, 827.
(43) Simons, G.; Parr, R. G.; Finlan, J. M. *J. Chem. Phys.* **1973**, *59*, 3229.
(44) Harding, L. B.; Ermler, W. C. *J. Comput. Chem.* **1985**, *6*, 13.
(45) Webster, B. C.; Buttar, D. *J. Chem. Soc., Faraday Trans.* **1992**, *88*, 1087.
(46) Wei, H. *Phys. Rev. A* **1990**, *42*, 2524; *J. Phys. B* **1990**, *23*, 2521.
(47) Rosen, N.; Morse, P. M. *Phys. Rev.* **1932**, *42*, 210; Manning, M. F.; Rosen, N. *Phys. Rev.* **1933**, *44*, 953.
(48) Kaur, S.; Mahajan, C. G. *Pramana J. Phys.* **1999**, *52*, 409.
(49) Kim, K.; Jordan, K. D. *Chem. Phys. Lett.* **1994**, *218*, 261.
(50) Mellor, W. E.; Kalotas, T. M.; Lee, A. R. *J. Chem. Phys.* **1997**, *106*, 6825.
(51) Macrae, R. M.; Briere, T. M. *Hyp. Int.* **1997**, *106*, 169.
(52) Cioslowski, J.; Scott, A. P.; Radom, L. *Mol. Phys.* **1997**, *91*, 413.
(53) Macrae, R. M.; Rhodes, C. J.; Briere, T. M.; Carmichael, I., manuscript in preparation.